Anomalous diffusion of multiple impurity species: Predicted implications for the ice core climate records

Alan W. Rempel[1] and J. S. Wettlaufer[2]
Applied Physics Laboratory, University of Washington, Seattle, Washington, USA

Edwin D. Waddington
Department of Earth and Space Sciences, University of Washington, Seattle, Washington, USA

Received 5 March 2002; revised 14 March 2002; accepted 17 July 2002; published 6 December 2002.

[1] We investigate the transport of impurities that are interpreted as climate proxies and are soluble in the premelted liquid that separates ice grains in the polar ice sheets even at subfreezing temperatures. Spatial variations in the relative abundances of multiple impurity species lead to gradients in their intergranular concentrations, defined as the ratio of the mass of dissolved impurity to the mass of premelted liquid. We show how diffusion down these intergranular concentration gradients affects anomalies in the bulk concentrations, defined as the ratio of the impurity mass to the mass of a polycrystalline sample, which are measured in polar ice cores. To illustrate these processes, we show that two initially asynchronous, periodic signals evolve to become in-phase after a short time: similar behavior is evident in coastal Antarctica, where there is a migration of methane sulfonate (MSA^-) from summer to winter peaks, and it becomes in-phase with the primary deposition of sea salt. Moreover, the approach allows us to examine how an initially constant bulk concentration profile is influenced by an abrupt change to the bulk concentration of a second component. The resulting profiles share features with those observed in the Eemian compositional record from the Greenland Ice Core Project (GRIP) ice core. *INDEX TERMS:* 1065 Geochemistry: Trace elements (3670); 1620 Global Change: Climate dynamics (3309); 1625 Global Change: Geomorphology and weathering (1824, 1886); 3670 Mineralogy and Petrology: Minor and trace element composition; 1827 Hydrology: Glaciology (1863); *KEYWORDS:* premelting, paleoclimate, segregation, soluble impurities, anomalous diffusion

Citation: Rempel, A. W., J. S. Wettlaufer, and E. D. Waddington, Anomalous diffusion of multiple impurity species: Predicted implications for the ice core climate records, *J. Geophys. Res.*, *107*(B12), 2330, doi:10.1029/2002JB001857, 2002.

1. Introduction

[2] Soluble impurity records that are retrieved from ice cores provide key evidence for past changes in atmospheric circulation [*Kreutz et al.*, 1997], marine productivity [*Legrand et al.*, 1997], volcanic activity [*Zielinski et al.*, 1997] and sea ice extent [*Welch et al.*, 1993]. When variations in the *bulk* concentration c_B of a given impurity (defined as the mass of the impurity divided by the mass of the core sample) are interpreted for their paleoenvironmental significance, it is usually assumed that the impurities have not moved relative to the ice with which they were originally deposited. However, careful analysis of the compositional records at high spatial resolution has shown that such relative motion does occur [e.g., *Wolff*, 1996]. For example, migration of methane sulfonate (MSA^-) has been detected in the firn, with peaks in bulk concentration moving from ice that was deposited (as snow) during past summers into ice that was deposited during past winters [*Pasteur and Mulvaney*, 2000]. The compositional record through the Eemian ice (deposited roughly 125–115 ka ago) in central Greenland at Greenland Ice Core Project (GRIP) reveals peculiar "shoulders" of diminished MSA^- and nitrate (NO_3^-) on either side of the peaks in bulk concentration [*Steffensen et al.*, 1997] that are found at depths where the integrity of the core stratigraphy has been questioned [*Alley et al.*, 1995]. Here we investigate how the transport of soluble impurities through unfrozen liquid can change the compositional records in glacial ice. Our goal is to quantitatively assess how processes that are fundamental to the phase behavior of polycrystalline ice can alter these climate proxies, with a view to further improving the reliability of ice core interpretations.

[3] The rate at which soluble impurities move depends critically on where the impurity molecules reside. In the next section, we discuss the available constraints on the local distribution of trace constituents at a given depth. This insight is used to develop a simple model for the transport of soluble impurities through the *premelted* liquid that lines the boundaries of the individual ice grains even at subfreez-

[1]Now at Department of Geology and Geophysics, Yale University, New Haven, Connecticut, USA.
[2]Now at Department of Geology and Geophysics and Department of Physics, Yale University, New Haven, Connecticut, USA.

0148-0227/02/2002JB001857$09.00

ing temperatures. When a single impurity species controls the liquid fraction, bulk impurity anomalies migrate relative to the ice in a shape-preserving manner at an anomalous velocity that is proportional to the temperature gradient [*Rempel et al.*, 2001a]. Here we show how this *anomalous diffusion* is modified when several dissolved species are present in the liquid. Motivated by the records in the ice cores, we demonstrate that diffusive transport can shift anomalies in the bulk concentrations of different impurity species relative to each other, and can also cause new ''sympathetic'' anomalies to form. We conclude by discussing the relevance of our predictions to the ice core records.

2. Impurity Locations

[4] At the time of deposition, the flux of snow and trace constituents to the surface of an ice sheet results in bulk impurity concentrations that reflect important aspects of the contemporary climate. After deposition, the degree to which transport processes affect the bulk impurity concentrations that are eventually measured from the ice cores depends on the distribution of impurities on a microscopic level. Of principal interest are the proportions of the impurities that are dissolved in unfrozen liquid under in situ conditions and the *intergranular* concentration c (defined as the mass of the dissolved impurity divided by the mass of the liquid) of each species in that aqueous solution. To motivate our modeling assumptions, we begin by reviewing the currently available direct observations of impurity locations. We then present thermodynamic arguments that further guide our expectations and help us to interpret the evidence for where the impurities reside.

2.1. Direct Observations

[5] Measurements of bulk impurity concentrations are typically made by analyzing the composition of meltwater derived from polycrystalline core samples; direct information on the in situ locations of the impurity molecules is lost. A few recent studies have attempted the difficult task of observing the partitioning of impurity molecules between the veins, grain boundaries and the exposed surfaces that were formerly at the interiors of single ice grains. The veins, which run along the triple junctions, form a liquid network that is connected via the nodes that define the locations where four grains meet [*Nye and Frank*, 1973]. To satisfy equilibrium requirements, the impurities that are detected in the vein network are assumed to have been dissolved in the liquid if the in situ temperature is above the eutectic temperature of their aqueous solution; for example, the eutectic temperature of NaCl in water is roughly 252 K and the eutectic temperature of H_2SO_4 solutions is 200 K. The surfaces of grain boundaries can be coated with liquid [*Raymond and Harrison*, 1975; *Ohtomo and Wakahama*, 1983], but they can also be dry, so it is uncertain whether impurities found at these locations were present in a concentrated solution or disseminated as solid precipitates. However, where the temperature exceeds the eutectic and concentrations of impurity molecules on grain boundaries are high, their presence might be regarded as evidence for local premelting. A few impurity species (F^-, Cl^-, and NH_3) can be bonded within the ice lattice, but most impurity molecules possess an excessive misfit strain energy [*Wolff*, 1996]. Accordingly, impurities that reside in grain interiors are assumed to be associated with dislocations or with larger inclusions such as dust particles. Interfacial premelting can cause dust particles to be coated with liquid films [*Rempel et al.* 2001b]; the role of dust as a potential impurity reservoir is discussed briefly later.

[6] Researchers from the British Antarctic Survey (BAS) used a scanning electron microscope (SEM) equipped with an energy-dispersive X-ray microanalysis facility to examine a sample of ice retrieved from just beneath the firn on Dolleman Island in Antarctica [*Mulvaney et al.*, 1988; *Wolff et al.*, 1988]. The sample was coated with a thin film of aluminum to avoid problems associated with the buildup of charge on the ice surface. The X-ray spectra, collected at 113 ± 4 K, revealed high concentrations of sulfur on the exposed surface expressions of veins. This was interpreted to indicate the presence of sulfuric acid at the in situ temperature of roughly 253 K. All of the H_2SO_4 detected in measurements of the melted sample could be accommodated in the vein network.

[7] *Fukazawa et al.* [1998] collected Raman spectra in polycrystalline samples from two Antarctic sites (Nansen ice and South Yamato ice). They probed veins located at various depths (4×10^{-6} to 8×10^{-3} m) beneath the sample surface. Examining 12 veins in the Nansen ice, they inferred that all of the sulfuric and nitric acid was present in the liquid network. The Raman spectra from the 3 veins examined in South Yamato ice indicated the presence of sulfate ions (SO_4^{2-}), but none of the hydrogen sulfate ions (HSO_4^-) that are expected when the intergranular concentration of H_2SO_4 is greater than about 0.1 M [*Wolff and Paren*, 1984]. Using this concentration as an upper bound and their estimated vein cross section of 2×10^{-12} m^2, together with the measured crystal size and bulk impurity concentration, they calculated that roughly 3% of the H_2SO_4 was present in the veins. No impurities were detected outside of the vein network; they indicated that this might reflect the fact that their technique is insensitive to ions contained in localized areas of less than about 10^{-12} m^2 in cross section.

[8] Groups at BAS and at Dartmouth College have independently pursued a variation of the SEM technique to obtain more detailed images of impurity locations. Instead of applying a conductive aluminum coating, the specimen is examined at a warmer temperature (150–213 K) so that its surface sublimates in the vacuum of the SEM chamber and charges are removed through vapor transport. In a series of recent papers [*Cullen and Baker*, 2000, 2001; *Baker and Cullen*, 2002] the Dartmouth group has reported on the impurity distributions they observed after the surface layers of ice from their samples were removed by sublimation at 253 K over periods ranging from a couple of hours to several weeks. High concentrations of impurity molecules, mainly Na and Cl, were found in filaments that traced the surface expressions of grain boundaries and veins. Isolated pockets of these species together with S, Mg, K, and Ca were detected in ''white spots'' on the exposed surfaces that were formerly in the grain interiors. Both the filaments and the highly concentrated white spots demonstrate the tendency of impurity molecules to coalesce while the water molecules sublimate away [see *Cullen and Baker*, 2001, Figure 1]. To limit both the potential for the redistribution of impurities as they coalesce, and the risk of contamination from the vapor phase, the group at BAS covered their

samples with a brass cap and quenched them in liquid nitrogen (boiling temperature 77 K) immediately after they were cleaved with a microtome blade [*Barnes et al.*, 2002a, 2002b]. They imaged similar features to those observed by the Dartmouth group, but had difficulty in detecting the impurity concentrations unless they waited a few minutes to allow several microns of ice to sublimate away. They report that some of the regions of high impurity concentration were associated with tiny dust particles; these were found both on the exposed surfaces of the individual ice grains and in the vicinity of grain boundaries.

[9] The techniques used to identify the precise locations of impurity molecules and measure their concentrations have become increasingly sensitive, yet further refinements are needed. A key issue, as noted by *Barnes et al.* [2002a], is the question of how the sample preparation affects the impurity locations that are ultimately observed. For example, the potential for surface or interfacial premelting [*Dash et al., al.*, 1995; *Wettlaufer*, 1999; *Worster and Wettlaufer*, 1999; *Wettlaufer and Dash*, 2000] to enhance the mobility of the impurity molecules on the exposed grain surface complicates the interpretation of the SEM results. As the direct observations do not yet provide a clear picture of the precise in situ distribution of impurity molecules, it will be necessary to make some assumptions for the modeling to progress in parallel with the refinement of experimental and field observational methodologies. Nevertheless, the available evidence shows that significant fractions of some impurity species are dissolved in the vein liquid. Molecular diffusion through this liquid network is the most rapid mode of transport. Hence, we need to determine the intergranular concentration of each impurity species to assess the magnitudes of the gradients that drive diffusion. We can then consider indirect evidence that helps to constrain the proportion of impurities that are dissolved in the liquid.

2.2. Equilibrium Considerations

[10] Thermodynamic arguments can be used to predict how the intergranular concentrations vary with depth. Common experience informs us that the presence of soluble impurities (e.g., salt) lowers the melting temperature of ice below the normal melting temperature of the bulk $T_m \approx 273$ K. Known as the *undercooling*, this depression of the equilibrium melting temperature is often described by a linear function [e.g., *Worster*, 2000] of the intergranular concentration c. For a single impurity species at a temperature T that is above the eutectic temperature of its aqueous solution, the undercooling is

$$T_m - T = \Gamma c, \tag{1}$$

where Γ is the slope of the liquidus curve. The Gibbs–Thomson effect modifies the undercooling at a curved solid-liquid interface by an amount proportional to the surface energy σ_{sl} so that

$$T_m - T = \Gamma c + \frac{T_m \sigma_{sl}}{\rho_s q_m} \mathcal{K}, \tag{2}$$

where ρ_s is the solid density, q_m is the latent heat of fusion per unit mass and the curvature $\mathcal{K}$ is defined to be positive when the solid–liquid interface is convex toward the liquid. Where the solid ice surface approaches a substrate such as a dust particle, the vapor phase, or another ice grain, equation (2) is generalized further to account for the effects of additional intermolecular interactions [e.g., *Wettlaufer*, 1999; *Rempel et al.*, 2001b].

[11] In the veins, we evaluate the relative importance of dissolved impurities and curvature effects by comparing the magnitudes of the different terms in equation (2). The curvature of the solid–liquid interface is inversely proportional to the vein radius R_v. We define the *characteristic radius* as

$$R_c \equiv \frac{T_m \sigma_{sl}}{\rho_s q_m (T_m - T)}, \tag{3}$$

and rearrange equation (2) to obtain

$$(T_m - T)\left(1 - \alpha \frac{R_c}{R_v}\right) = \Gamma c, \tag{4}$$

where α is a constant of order unity that depends on the detailed vein geometry [e.g., *Mader*, 1992a]. If the vein radius is much greater than the characteristic radius, then equation (4) indicates that the effects of interfacial curvature are negligible; equilibrium is achieved by adjusting the mass fraction of liquid so that the intergranular concentration is related directly to the undercooling, and equation (1) is satisfied.

[12] In the polar ice cores the characteristic radius is typically only a few nanometers (e.g., with $\sigma_{sl} \approx 0.035$ J/m^2, $\rho_s \approx 10^3$ kg/m^3, and $q_m \approx 3.3 \times 10^5$ J/kg, equation (3) gives $R_c \approx 3 \times 10^{-9}$ m when $T \approx 263$ K). The measurement resolution quoted by *Fukazawa et al.* [1998] suggests that the vein radii in their samples were approximately 3 orders of magnitude larger than R_c; this is a strong indication that the intergranular concentrations are directly related to the undercooling. Additional support for this conjecture is provided by the qualitative observations of elevated impurity concentrations in the vicinity of veins. Geometrical arguments show that the volume fraction of liquid contained in the veins is proportional to the square of the ratio between the vein radius and the grain size b. The liquidus concentration at ice core temperatures is typically of order 1 M; this sets an upper bound on the intergranular concentration. If the vein radius were comparable to the characteristic radius, then the largest proportion of impurities that could be dissolved in the vein liquid would be approximately $(R_c/b)^2$ (c/c_B), which is of order 10^{-6} under typical conditions (e.g., with $R_c \approx 10^{-9}$ m, $c_B \approx 10^{-6}$ M, and $b \approx 10^{-3}$ m). Since the direct evidence [*Fukazawa et al.*, 1998; *Mulvaney et al.*, 1988; *Wolff et al.*, 1988; *Cullen and Baker*, 2000, 2001; *Baker and Cullen*, 2002; *Barnes et al.*, 2002b] indicates that a much larger fraction of the impurities is located in the veins, we conclude that $R_v \gg R_c$. Hence, we can deduce the intergranular concentrations in the veins directly from the measured in situ temperature profile. In the following, we assume that all the liquid at a given depth is in compositional equilibrium, so that the intergranular concentration in the veins is the same as the intergranular concentration in any other liquid that is present, for example on grain boundaries.

[13] Thus far we have focused on the case in which a single impurity species is dissolved within the premelted liquid. When several species are present, the equilibrium

temperature of the melt is influenced by the intergranular concentration of each component. We approximate the phase behavior using a linear combination of the intergranular concentrations c_i so that, with $R_v \gg R_c$, the generalized form of equation (4) is

$$T_m - T \approx \sum_{i=1}^{N} \Gamma_i c_i, \tag{5}$$

where Γ_i is the liquidus slope for the ith component, and a total of N components are dissolved in the melt. Equation (5) is valid for the small changes in intergranular concentration and temperature on which we focus in this work. More accurate, nonlinear chemical-thermodynamic models for certain aqueous solutions are available [e.g., *Marion and Grant*, 1994], but this linear approximation is more useful for providing intuition into the dynamics of the transport processes that affect the bulk impurity records. At fixed temperature, the intergranular concentration of the ith component depends on the relative availability of the other impurity species.

[14] We make use of indirect evidence to guide our assumption for what proportion of the total impurity content is dissolved in the liquid network. The distribution coefficient k is defined as the ratio of the equilibrium impurity concentration in the solid to the equilibrium impurity concentration in the liquid c; k is generally treated as a constant. Assuming that the impurities are partitioned at equilibrium between the liquid and the solid, we write the bulk concentration as

$$c_B = \phi c + k(1-\phi)c \approx (\phi + k)c, \tag{6}$$

where $\phi \ll 1$ is the mass fraction of liquid present. If the distribution coefficient is much smaller than the liquid mass fraction, then equation (6) implies that most of the impurities are dissolved within the liquid. The sizes of the ice grains are anticorrelated with the bulk impurity concentrations through most of the depth of the polar cores [*Thorsteinsson et al.*, 1997; *de la Chapelle et al.*, 1998]. Curvature effects should cause the vein radii to be roughly uniform [*Mader*, 1992a, 1992b; *Nye*, 1992], so variations in grain size imply variations in the liquid fraction, with larger grains corresponding to smaller ϕ. The observed spatial variations in grain sizes and bulk impurity concentrations occur over much shorter length scales than do changes in the intergranular concentrations inferred from the gradual variations in temperature along the core. Hence, the variation in liquid fraction implied by the observed grain-size distribution is consistent with equation (6) only if $\phi \gg k$, a point to which we return later; however, this sets the stage for our model of impurity transport with

$$c_B \approx \phi c. \tag{7}$$

Toward the end of the paper, we relax this assumption and retain a finite value for k in equation (6) in order to examine how the transport is changed when an appreciable fraction of the impurities is excluded from the liquid phase. When several species are present, the appropriate generalization of equation (7) for the ith impurity species is

$$c_{Bi} \approx \phi c_i. \tag{8}$$

As the values of Γ_i are generally most similar when the concentration is expressed in terms of the molar concentration, this system of units will prove most convenient in the examples that follow. When using the molar concentration instead of the mass fraction, this implies a change of definition for ϕ from the mass fraction of liquid to the volume fraction of liquid (porosity); the two are numerically almost equivalent.

3. Impurity Transport

[15] The transport of impurities must satisfy conservation laws; any change in the mass of the ith impurity species contained within an arbitrary volume V is compensated by advection and diffusion of that species across the bounding surface S. We treat the polycrystalline ice matrix as a continuum with a uniform local velocity $\mathbf{v}$ (i.e., the ice sheet flow velocity). Scaling arguments show that fluid velocities are low enough that the advective flux of impurities through the veins is negligible in comparison to the (Fickian) diffusive flux through the liquid [*Rempel*, 2000], and hence the mass balance for the ith species is written as

$$\frac{\partial}{\partial t}\int_V c_{Bi}\mathrm{d}V = -\oint_S (c_{Bi}\mathbf{v} - D_i\phi\nabla c_i) \cdot \mathrm{d}\mathbf{S}, \tag{9}$$

where D_i is the diffusion coefficient and ϕ includes all the connected liquid through which diffusion progresses. To account for the fact that the transport paths (veins) are randomly oriented with respect to the prevailing concentration gradient, we follow *Nye* [1991] and adopt a value for D_i equal to one-third the normal molecular diffusivity of the impurity in water. It is then convenient to define an anomalous velocity as

$$\mathbf{v}_{ci} = -D_i \frac{\nabla c_i}{c_i}, \tag{10}$$

so that equation (8) implies that $-D_i\phi\nabla c_i = c_{Bi}\mathbf{v}_{ci}$; the anomalous velocity can be thought of as a measure of the speed with which bulk impurity anomalies migrate relative to the surrounding ice. We apply the divergence theorem to the right side of equation (9) and note that the integrands of the resulting equation must balance since the volume V is arbitrary. Treating the ice crystals themselves as incompressible (i.e., $\nabla \cdot \mathbf{v} = 0$), we obtain [*Rempel et al.*, 2001a]

$$\frac{\partial c_{Bi}}{\partial t} + \mathbf{v} \cdot \nabla c_{Bi} = -\nabla \cdot (\mathbf{v}_{ci} c_{Bi}) . \tag{11}$$

The left side of equation (11) is the material derivative of the bulk concentration of the ith impurity species; this is the net change in bulk concentration within a moving ice parcel. Since the right side of the equation, involving the anomalous velocity, is nonzero, equation (11) describes how bulk impurity anomalies evolve. To understand the characteristics of this evolution, first we need to express the anomalous velocities in terms of the bulk concentrations and the temperature, parameters that are routinely measured during ice coring studies.

[16] We combine equations (5) and (8) to write the undercooling as a function of the N different bulk concen-

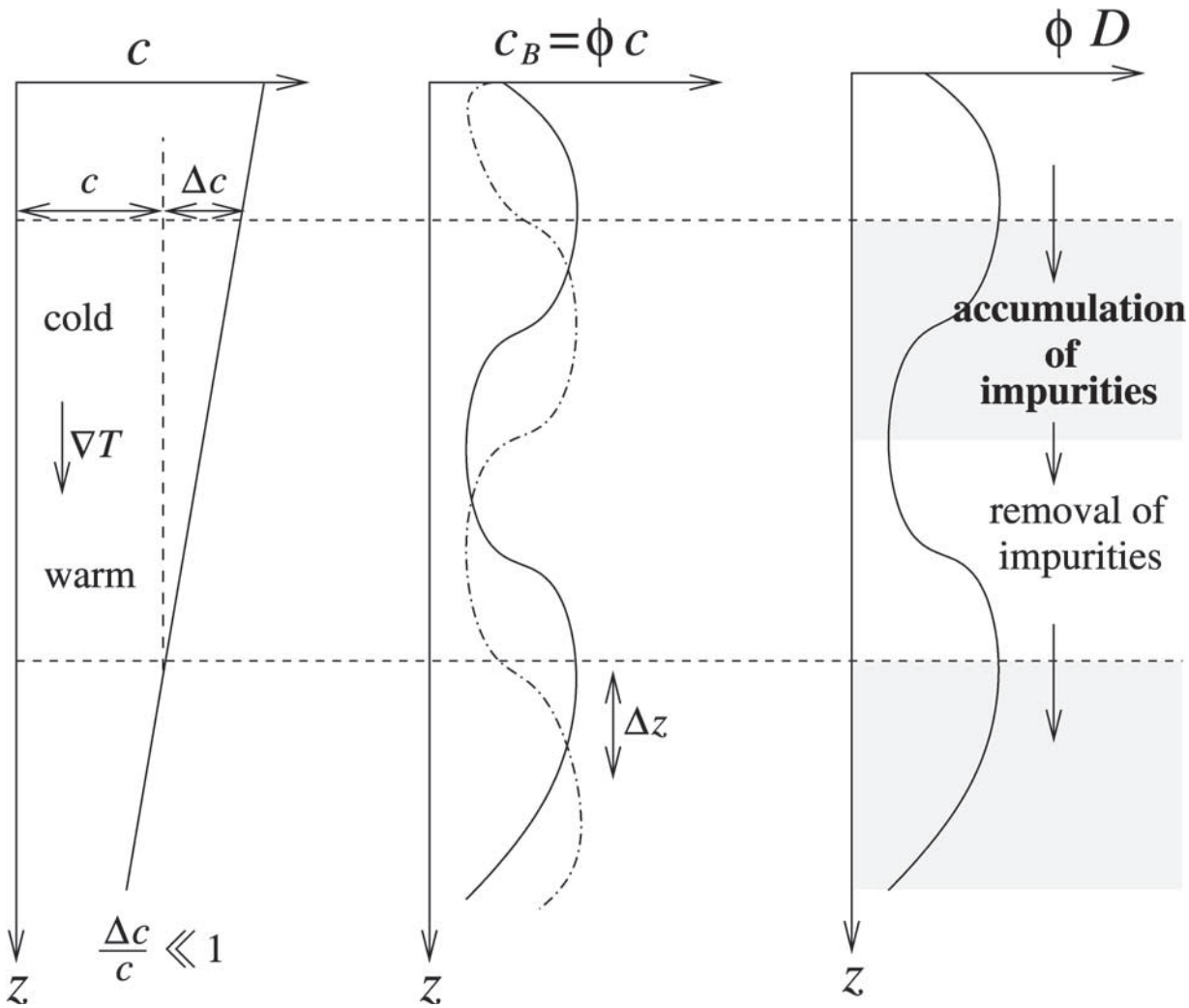

Figure 1. The physical interactions that cause molecular diffusion to translate the c_B-profile in a shape-preserving manner when the intergranular concentration depends only on the local temperature (modified from the work of *Rempel et al.* [2001a]. The temperature varies gradually with depth so that the relative change in the intergranular concentration $\Delta c/c$ is small over short distances, as shown in the panel on the left. The solid line in the middle panel represents a segment of the c_B-profile, which experiences much more abrupt spatial variations. Because c is relatively constant, the variation in c_B is associated with rapid changes in liquid fraction ϕ. The rightmost panel reflects how the effective diffusivity ϕD mirrors the fluctuations in c_B so that the rate of diffusive solute transport $\phi D \nabla c$, as described by equation (9), is fastest where c_B is greatest. The rate of transport into the shaded regions is greater than the rate of transport out of those regions and this allows impurities to accumulate. The intergranular concentration is fixed by the thermal field, but ϕ adjusts so that the peaks and troughs in the c_B-profile are translated relative to the ice matrix. The bulk concentration has moved a distance $\Delta z = \mathbf{v}_c \Delta t$ with its shape unaltered after a time Δt, as shown by the dot-dashed line in the middle panel.

trations and the intergranular concentration of the ith impurity species as

$$T_m - T = \frac{c_i}{c_{Bi}} \sum_{j=1}^{N} \Gamma_j c_{Bj} \; . \tag{12}$$

This allows us to write the gradient of c_i, which drives compositional diffusion through the liquid, as

$$\nabla c_i = \frac{\nabla (T_m - T)}{\frac{1}{c_{Bi}} \sum \Gamma_j c_{Bj}} - \frac{(T_m - T) \nabla \left(\frac{1}{c_{Bi}} \sum \Gamma_j c_{Bj} \right)}{\left(\frac{1}{c_{Bi}} \sum \Gamma_j c_{Bj} \right)^2}, \tag{13}$$

where the summations are made over j from 1 to N. The two terms on the right side of equation (13) account for the contributions to the intergranular concentration gradients that are produced by gradients in temperature and by gradients in the chemical loading. Using equations (12) and (13) to rewrite equation (10) for the anomalous velocities, we find that

$$\mathbf{v}_{ci} = D_i \frac{\nabla T}{T_m - T} + D_i \frac{\sum \Gamma_j \nabla c_{Bj} - \frac{\nabla c_{Bi}}{c_{Bi}} \sum \Gamma_j c_{Bj}}{\sum \Gamma_j c_{Bj}}, \tag{14}$$

which shows how the anomalous velocities depend on the measured quantities.

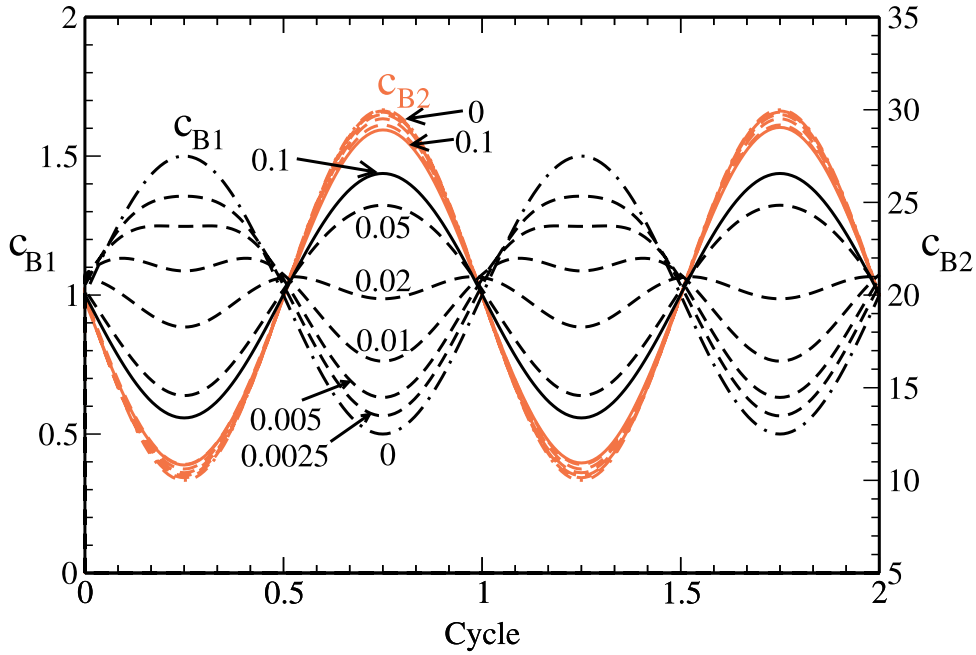

Figure 2. The evolution of periodic c_{Bi}-profiles that were deposited asynchronously on the surface of an ice sheet; the initial profiles are the dot-dashed lines marked "0." The c_{B1}-profiles, shown in black, have much lower concentrations than the c_{B2}-profile, shown in red; note the different vertical scales. When the vertical axes are measured in units of micromoles per liter, the amplitudes of the c_{B1} and c_{B2} fluctuations are comparable to those of the MSA^- and Na^+ fluctuations observed in the Dolleman Island ice core [*Pasteur and Mulvaney*, 2000]. The horizontal axis represents the distance along the core, measured in terms of the period of the anomaly cycle, which can be thought of as the annual layer thickness (typically tens of centimeters). The dashed lines show the profiles at the subsequent times, labeled on the c_{B1}-profiles in terms of the diffusion timescale, as described in the text. The solid lines show that the low-amplitude c_{B1}-profile is in phase with the c_{B2}-profile after a dimensionless time of 0.1. The c_{B2}-profile is not significantly altered.

[17] If the liquid contains only a single impurity species, the second term on the right side of equation (14) is equal to zero, and the anomalous velocity is directly proportional to the temperature gradient. Thermal diffusion rapidly smooths temperature gradients so that the temperature variations that produce gradients in intergranular concentration generally occur over much broader length scales than do variations in bulk concentration. This implies that when the anomalous velocity is proportional to ∇T, as in this simple case, $\mathbf{v}_{ci}$ changes gradually in comparison to changes in c_{Bi} (i.e., $c_{Bi}\,\nabla\cdot\mathbf{v}_{ci} \ll \mathbf{v}_{ci}\cdot\nabla c_{Bi}$) and equation (11) describes how the bulk concentration profile is translated relative to the ice in a shape-preserving manner (see Figure 1). The same behavior is expected when several impurity species are in aqueous solution and their relative proportions are uniform, as equation (14) can be simplified to show that $\mathbf{v}_{ci}$ is directly proportional to ∇T for this case too. The bulk concentrations of many species tend to covary along the ice cores, so anomalous diffusion should often be characterized by the same gradual, shape-preserving migration of the c_{Bi}-profiles that was predicted for the single impurity case. However, when the relative proportions of the dissolved species vary with depth, the second term on the right side of equation (14) is significant, and $\mathbf{v}_{ci}$ and c_{Bi} change appreciably over similar length scales. This causes different parts of each bulk concentration anomaly to move at different rates, so that the shapes of the individual c_{Bi}-profiles are altered. To focus on these effects we restrict our attention to isothermal ice in the examples that follow, and we neglect the effects of layer thinning due to ice sheet flow. This approach is justified by the observations of $T(z)$, which show gradual variations over the length scales of interest (e.g., see Figure 1).

3.1. Shifting Periodic Signals

[18] First we examine the case in which two components are present in solution, and the initial c_{Bi}-profiles are characterized by periodic spatial variations that are 180° out-of-phase, as shown by the dot-dashed lines in Figure 2. In addition, the bulk concentration of one component (species 2) is much greater than the bulk concentration of the other component (species 1, note the different scales on the figure). For an isothermal system with two components, equation (14) for the anomalous velocities can be manipulated to show that

$$\mathbf{v}_{c1} = D_1\Gamma_2\frac{\nabla c_{B2} - \frac{c_{B2}}{c_{B1}}\nabla c_{B1}}{\Gamma_1 c_{B1} + \Gamma_2 c_{B2}}, \tag{15}$$

$$\text{and}\quad \mathbf{v}_{c2} = D_2\Gamma_1\frac{\nabla c_{B1} - \frac{c_{B1}}{c_{B2}}\nabla c_{B2}}{\Gamma_1 c_{B1} + \Gamma_2 c_{B2}} = -\frac{D_2\Gamma_1 c_{B1}}{D_1\Gamma_2 c_{B2}}\mathbf{v}_{c1}\ , \tag{16}$$

where the diffusion coefficients D_1 and D_2 are similar in size, as are the constants Γ_1 and Γ_2. Equation (16) indicates

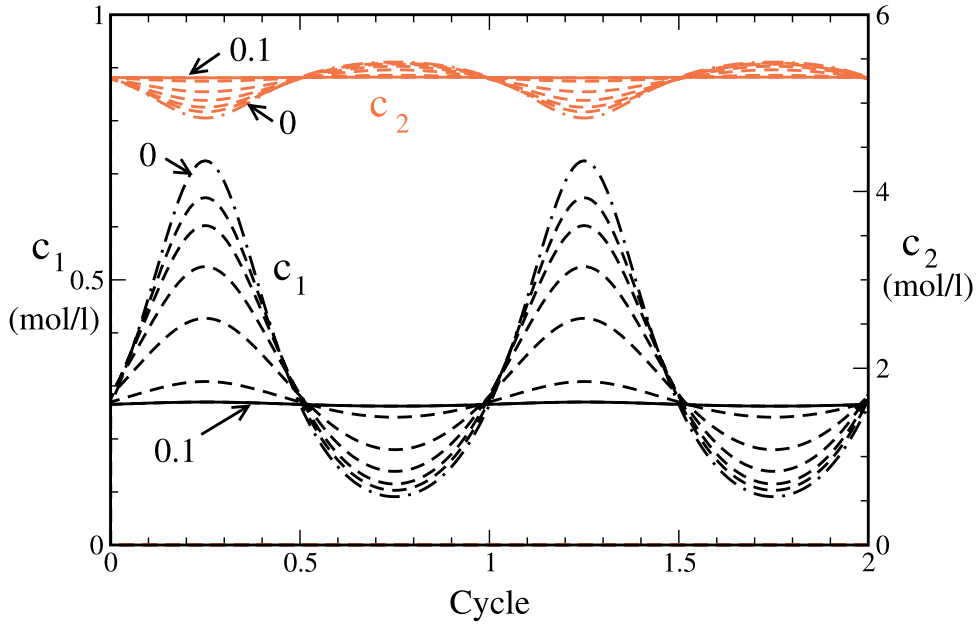

Figure 3. The intergranular concentration profiles that correspond to the bulk concentration profiles shown in Figure 2, calculated using an undercooling of $T_m - T = 20$ K, with $\Gamma_1 = \Gamma_2 = 3.6$ K/M. Over time, both profiles evolve so that the peak concentrations in the liquid are reduced in amplitude and near-constant levels are attained.

that the ratio of the anomalous velocities depends on the ratio of the two bulk concentrations; accordingly, we expect the shape of the anomaly for the component with the lower bulk concentration (species 1) to change much more rapidly than the shape of the anomaly for the component with the higher bulk concentration (species 2). This behavior reflects the relative importance of the two components in influencing the total liquid fraction.

[19] If the wavelengths of the initial profiles correspond to the thickness of an annual layer, then the diffusion timescale is defined as $\tau = \lambda^2/D$, where λ is the layer thickness and D is the diffusion coefficient, which is taken to be equal for both species. The dashed lines in Figure 2 show the evolution of the two bulk concentration profiles, plotted at different times $\tilde{t}$ measured in units of this diffusion timescale. With $\lambda = 0.4$ m and $D = 5 \times 10^{-10}$ m^2/s, $\tau \approx 10$ years and the lines marked with 0.1 correspond to the predicted profiles one year after diffusive transport began. The low-amplitude c_{B1}-profile rapidly changes shape. The initial c_{B1}-peaks diminish in strength and reemerge at the former locations of the c_{B1}-troughs so that the entire profile becomes in-phase with the variations shown in the c_{B2}-profile. In contrast, the c_{B2}-profile experiences only a minor reduction in amplitude over the same time period. By $\tilde{t} = 0.1$, the two profiles are in-phase, and integrations until later times yield no significant further alterations.

[20] At first it may seem counterintuitive that diffusive transport acts to shift and reestablish concentration peaks rather than to cause their dispersal. The physical interactions that are responsible for this behavior are made more transparent by considering the evolution of the intergranular concentration profiles, which can be found from equation (12). Figure 3 shows the intergranular concentrations that correspond to the bulk concentrations displayed in Figure 2. Initially, the intergranular concentration profiles are periodic and out-of-phase, much like the c_{Bi}-profiles. The relatively large liquid fraction associated with bulk concentration peaks of the dominant species (species 2) causes local dilution of the minor species (species 1) in the liquid. Diffusion drives both species to even out their concentrations in the liquid. For the minor species, this results in the relocation of the bulk concentration peaks, eventually achieving a steady state. For the dominant species the effects of impurity transport are much less pronounced because the initial intergranular concentration profile is relatively smooth and the relocation of only a small proportion of the impurity molecules is required to establish compositional equilibrium.

[21] This simple system can be viewed as an analog for the alteration to the MSA^- profile that has been observed at several coastal Antarctic stations [*Pasteur and Mulvaney*, 2000]. While methane sulfonic acid, with a eutectic temperature of approximately 198 K in aqueous solution, is deposited primarily in the summer because of its association with oceanic biological activity, peaks in the recorded bulk concentration of MSA^- are found to coincide with the isotopic winter once the ice reaches several tens of meters depth. Another prominent impurity species with a relatively low eutectic temperature (252 K) is NaCl, which is derived from sea salt that is deposited at peak concentrations during the winter months. The bulk concentrations of NaCl that are deposited in these coastal locations are always many times greater than the bulk concentrations of MSA^-. If both species are present in the premelted liquid, then the relocation of MSA^- can easily be explained by the mechanism described here. *Pasteur and Mulvaney* [2000] note that the relocation is not directly related to depth below the surface or to time since deposition. Our calculations indicate that relocation could be accomplished by anomalous diffusion in as short a time as a single year. We speculate that the

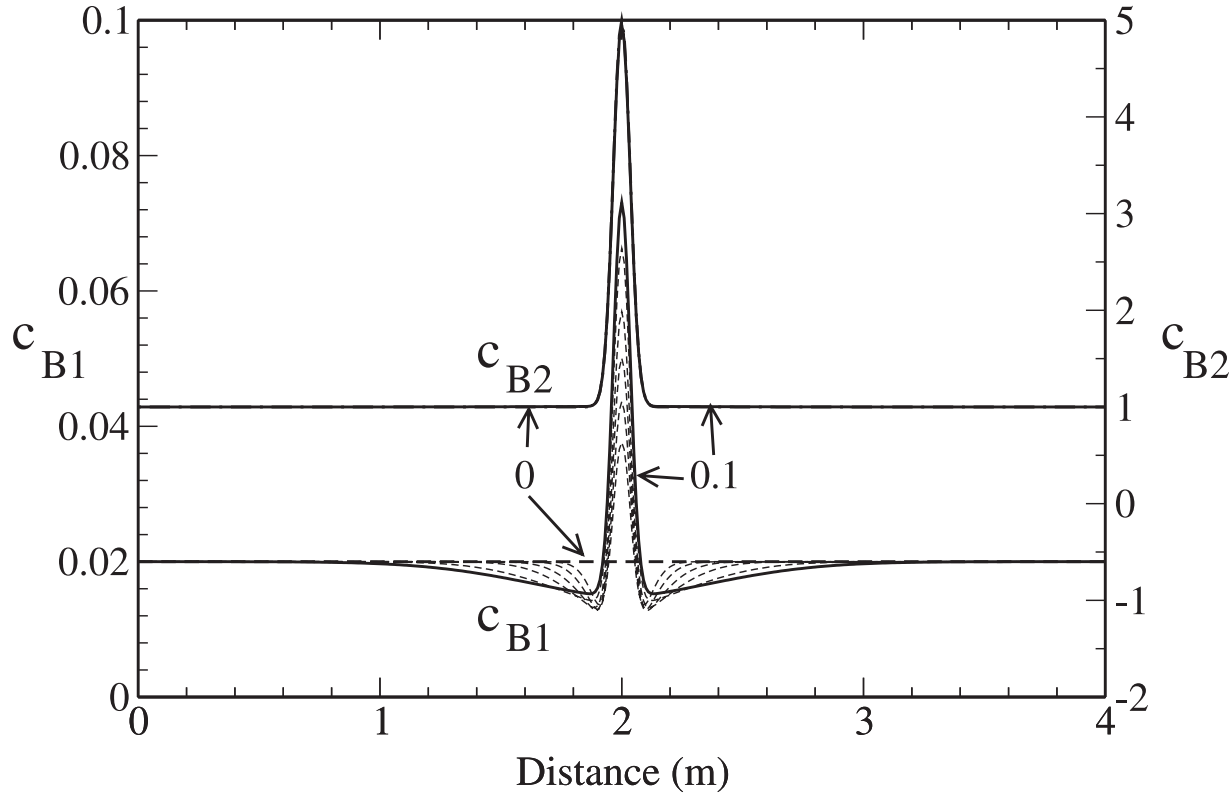

Figure 4. The change in an initially constant c_{B1}-profile in response to a Gaussian spike in the c_{B2}-profile. The dot-dashed lines represent the initial signals and the dashed lines show the evolution of these signals at the same dimensionless time steps that are plotted in Figures 2 and 3. The solid lines show the profiles after 0.1 dimensionless time units. The c_{B2}-profile is barely altered, but the c_{B1}-profile develops a matching Gaussian spike, bordered on each side by a region of reduced concentration. When the concentrations are measured in micromoles per liter, the amplitudes and shapes of the c_{B1} and c_{B2} signals are similar to those of the MSA^- and SO_4^{2-} signals in Eemian isotopic event 1 at GRIP [*Steffensen et al.*, 1997].

variable timing observed in the ice core record might be caused by a delay in establishing the connected liquid networks, due for example to variations in the accumulation rate, that are required for transport to progress. The changes to the MSA^- profiles take place in the firn, where the interruption of the vein network by air bubbles, for example, might slow the rate of impurity transport. We emphasize, however, that what the theory shows is that compositional diffusion alone can produce the observed signal alterations without invoking any additional physical processes, such as irreversible chemical interactions.

3.2. Sympathetic Bulk Concentration Spikes

[22] Next we examine how an initially constant c_B-profile responds to abrupt spatial variations in the bulk concentration of a second impurity species. In Figure 4 the evolution of two bulk concentration profiles is shown at the same dimensionless time steps as in Figure 2. Initially, c_{B1} is uniform at 2×10^{-8} M and the c_{B2}-profile contains a Gaussian spike. Figure 5 shows how the increased liquid fraction that is associated with the abrupt rise in c_{B2} produces an extremely low local concentration of species 1 in the liquid. The gradient in c_1 drives compositional diffusion and leads to the rapid development of a "sympathetic" spike in the c_{B1}-profile. The bulk concentration on both sides of the spike is depleted in order to supply the species 1 material to the region of the sympathetic spike. The c_{B2}-profile undergoes little change, with a slight reduction in amplitude and a nearly imperceptible broadening near the edges of the spike. The solid curves show the profiles after $\tilde{t} = 0.1$. At later times, the depressions in c_{B1} that formed near the spike are slowly replenished from further away as the intergranular concentrations equilibrate. Additional calculations show that the c_{B2}-profile experiences more significant changes when the two species have more similar initial bulk concentrations, but the general features produced by anomalous diffusion remain the same. The bulk concentrations evolve to achieve a steady state in which their ratio is spatially uniform.

[23] The regions of depleted concentration in the c_{B1}-profile are reminiscent of the "shoulders" of reduced MSA^- and NO_3^- found on both sides of coincident peaks in the bulk concentrations of most impurity species located within the Eemian isotopic events at GRIP. The atmospheric gases preserved in the Eemian events suggest that the stratigraphy has been disrupted and that the ice derives from a different climate epoch [*Chappellaz et al.*, 1997]. However, the compositional signatures of these events are markedly different from any observed in the rest of the core, an observation that has been used to argue against ice

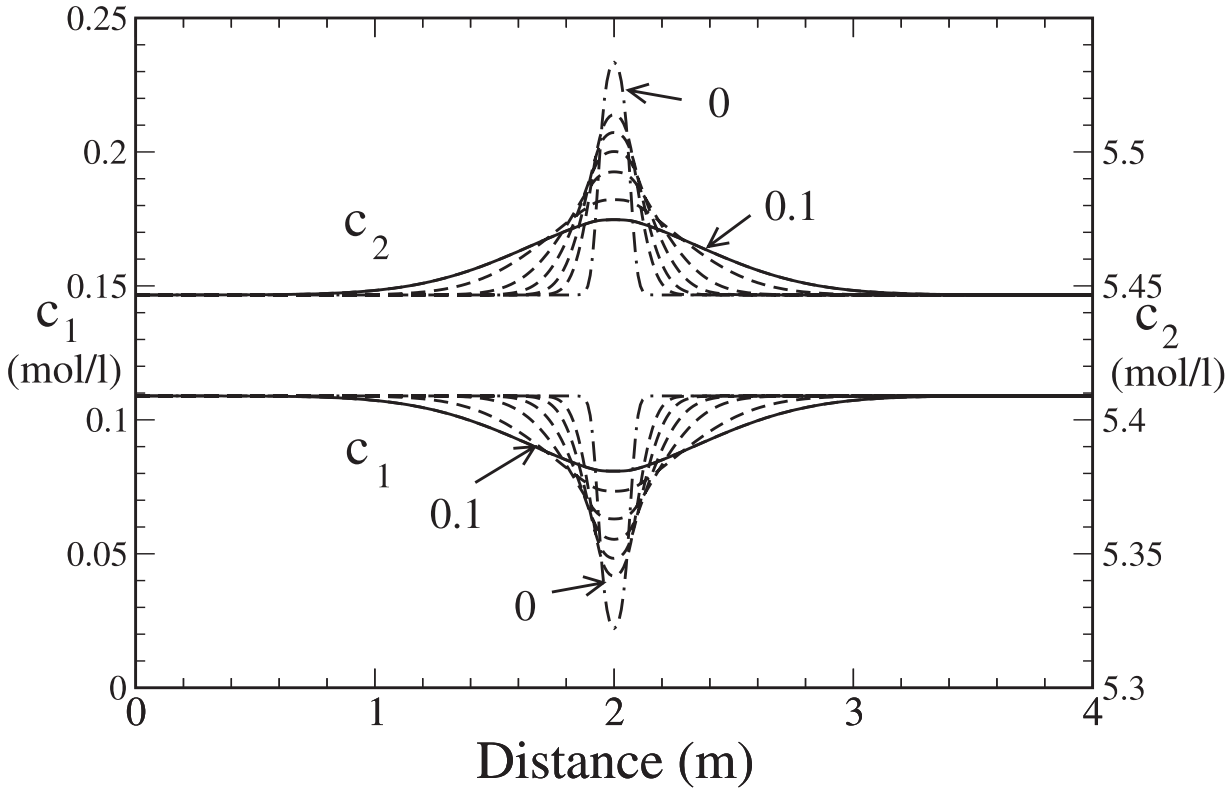

Figure 5. The intergranular concentration profiles that correspond to the bulk concentration profiles shown in Figure 4, calculated using an undercooling of $T_m - T = 20$ K, with $\Gamma_1 = \Gamma_2 = 3.6$ K/M. The peak in the bulk concentration of species 2 is associated with an increased liquid fraction that dilutes the intergranular concentration of species 1 so that diffusion leads to the formation of the sympathetic anomaly shown in Figure 4. Meanwhile, species 2 experiences an intergranular concentration gradient that drives diffusion outward, leading to a slight broadening of the initial peak.

injection [*Steffensen et al.*, 1997]. The results presented here suggest that the compositional record may have been significantly altered following an injection event. The width of the Gaussian spike in Figure 4 roughly corresponds to that of Eemian event 1 at GRIP, and, using the same diffusivity as before, this implies a timescale τ of less than a century. The "shoulders" in the c_{B1}-profile, shown in Figure 4, are significantly diminished after just a fraction of this time period. However, inferences based on the observed diffusion of the isotopic signal [*Johnsen et al.*, 1997] constrain the injection event to have occurred some ten to twenty thousand years in the past. One cannot exclude the possibility that complex, flow-induced mixing processes, such as recumbent folding or shear-zone formation, may be responsible for generating these peculiar signals [e.g., *Souchez et al.*, 1995; *Souchez*, 1997; *Waddington et al.*, 2001]. Clearly, the model we have presented so far is inadequate to fully explain the chemical profiles that derive from the Eemian ice at GRIP. This discrepancy prompts us to revisit, among other things, our assumption that the impurities are confined mainly to a connected liquid network.

3.3. The Effect of Partitioning

[24] Distribution coefficients themselves, as used in equation (6), depend on a variety of thermodynamic state variables and the degree of physical and chemical disequilibrium [e.g., *Tiller*, 1991, p. 131], and are not generally known for multiple-component aqueous solutions. Indeed, laboratory solidification experiments used to infer the distribution coefficient [e.g., *Gross and Svec*, 1997, and references therein] represent only an upper bound [*Wettlaufer*, 1998]. Moreover, the "effective" distribution coefficients for such a homogenized model as we develop here depend on the geometry of the phase boundaries and the nature of the interfaces themselves. For example, the volume fraction of liquid contained in veins is proportional to the square of the ratio between the vein radius R_v and the grain size b, while the surface area of grain boundaries in a representative volume of ice is inversely proportional to b. If the impurities are less mobile on the grain boundaries than in the veins, either because of confinement or because of the formation of precipitates, and their surface concentration is proportional to the intergranular concentration in the veins, then at equilibrium the effective distribution coefficient can be inversely related to the grain size. Similarly, when a significant proportion of the impurities is present on the surfaces of insoluble particles, such as dust, then the distribution coefficient is expected to vary in proportion to the particle volume fraction (assuming the particle-size distribution is spatially uniform). Indeed, even for a solution with a lower eutectic temperature than is experienced in situ, it is plausible that a significant propor-

tion of the impurities may be outside the liquid network, especially in "dirty" ice, such as that which corresponds to the GRIP Eemian isotopic events.

[25] In the models of impurity transport developed so far, we have assumed that most of the soluble impurities are dissolved in a connected liquid network where the liquid fraction is always much greater than the distribution coefficient, so that $\phi \gg k$ in equation (6). To examine the way in which the effects of anomalous diffusion are slowed when a significant proportion of the impurities is not in this liquid phase, we assume that the impurities are partitioned at equilibrium, and we replace equation (8) by

$$c_{Bi} \approx (\phi + k_i) c_i \ , \tag{17}$$

where k_i is the distribution coefficient for the ith impurity species. This equation is valid when the impurities reach an equilibrium distribution more quickly than the concentration in the liquid changes. The solute conservation is still described by equation (11), but with the generalized anomalous velocities defined by

$$\mathbf{v}_{ci} = -D_i \frac{\nabla c_i}{c_i} \frac{\phi}{\phi + k_i} = -D_i \frac{\nabla c_i}{c_i} \left(1 - \frac{k_i c_i}{c_{Bi}}\right) . \tag{18}$$

The anomalous velocity is higher where the liquid fraction is greater and a larger proportion of the impurities are in solution. Equation (5) can be combined with equation (17) to obtain

$$T_m - T = c_i \sum_{j=1}^{N} \frac{\Gamma_j c_{Bj}}{c_{Bi} + c_i (k_j - k_i)} \ , \tag{19}$$

which represents a set of N coupled equations for the N unknown intergranular concentrations c_i. Equations (18) and (19) apply quite generally, even when the distribution coefficients vary spatially.

[26] We examine the special case in which the differences between the distribution coefficients are small (i.e., $k_j - k_i \ll k_i$) so that the second term in the denominator of equation (19) is negligible. This allows us to express the anomalous velocity for the ith species as

$$\mathbf{v}_{ci} = D_i \left(\frac{\nabla T}{T_m - T} + \frac{\sum \Gamma_j \nabla c_{Bj} - \frac{\nabla c_{Bi}}{c_{Bi}} \sum \Gamma_j c_{Bj}}{\sum \Gamma_j c_{Bj}} \right) \times \left[1 - \frac{k_i (T_m - T)}{\sum \Gamma_j c_{Bj}} \right] , \tag{20}$$

which is a multiple of equation (14), where the scaling factor in square brackets is equal to $\phi/(\phi + k_i) \leq 1$. In isothermal ice, the anomalous velocities are still zero where the bulk concentrations covary. When the distribution coefficients are of similar size, the same steady state bulk impurity profiles are achieved regardless of whether or not the majority of the impurities are in the liquid phase. However, as the distribution coefficients are increased, the anomalous velocities are reduced and it takes more time to achieve a steady state. Moreover, since the anomalous velocities are generally faster where the liquid fraction is greater, the evolution toward a steady state occurs at different rates along the anomaly profile.

[27] To see how this alters the characteristics of the formation of a sympathetic spike, in Figure 6 we reexamine the evolution of an initially constant c_{B1}-profile that interacts with a Gaussian spike in c_{B2}. The distribution coefficients were both chosen to be equal to one hundred times the minimum initial liquid fraction $\phi|_{min}$ outside the Gaussian spike in the c_{B2}-profile. If the bulk concentrations are measured in micromoles per liter, the undercooling is roughly 20 K and $\Gamma_1 = \Gamma_2 \approx 3.6$ K/M, then this implies that $\phi|_{min} \approx 10^{-9}$ and $k_1 = k_2 \approx 10^{-7}$. The c_{B1}-profile is predicted to evolve much more slowly than when all the impurities are confined to the liquid phase, as can be seen by comparison with Figure 4; the "shoulders" on the edges of the sympathetic spike persist even when $\tilde{t} = 10$, which corresponds to a time interval of roughly 1000 years. The choice of distribution coefficients could be "tuned" to produce an evolution time that corresponds to that inferred from the isotopic data by *Johnsen et al.* [1997] for the Eemian event, but such an exercise is purely demonstrative of potential controlling effects. Additional complications are likely to arise; it is worthwhile to note, for example, that the bulk impurity concentrations do not covary at steady state when the distribution coefficients are dissimilar in size.

[28] Anomalous diffusion is not the only physical process that can cause the postdepositional alteration of the c_{Bi}-profiles and influence the anomalies that are observed in the polar ice cores. Other effects, such as the precipitation of insoluble salts, the migration of dust particles by thermal regelation [*Rempel et al.*, 2001b] and irreversible chemical reactions, undoubtedly affect the preservation of the detailed chemical records to some extent. In addition, complex ice deformation processes can also alter the core stratigraphy [*Souchez et al.*, 1995; *Souchez*, 1997; *Waddington et al.*, 2001]. Further efforts to quantify such changes will promote increased confidence and improved understanding of the integrity of these valuable, and difficult-to-obtain, climate records. Refinements to, and extensions of the model that we have presented here will benefit from a more well-developed understanding of such matters as the phase equilibria for the complex mixtures of impurity species that are deposited on the polar ice sheets, and the liquid volume fractions and effective partition coefficients within naturally occurring glacier ice. Research into these areas is necessary to promote a fuller understanding of paleoenvironmental change.

4. Conclusions

[29] Diffusion of soluble impurities through the small volumes of premelted liquid that are at equilibrium in ice sheets can significantly affect the bulk concentration profiles that are measured in ice cores. The intergranular concentration gradients that drive diffusive transport are caused by gradients in the temperature and by gradients in the chemical loading. When most of the impurities are confined to the liquid network, our models predict that the bulk concentrations of different species adjust so that their ratios become spatially uniform. This behavior can explain the migration of MSA^- so that, several years after deposition during the Antarctic summer, the peaks in bulk concentration adjust to coincide with the elevated bulk concentrations of sea salt that were originally deposited at

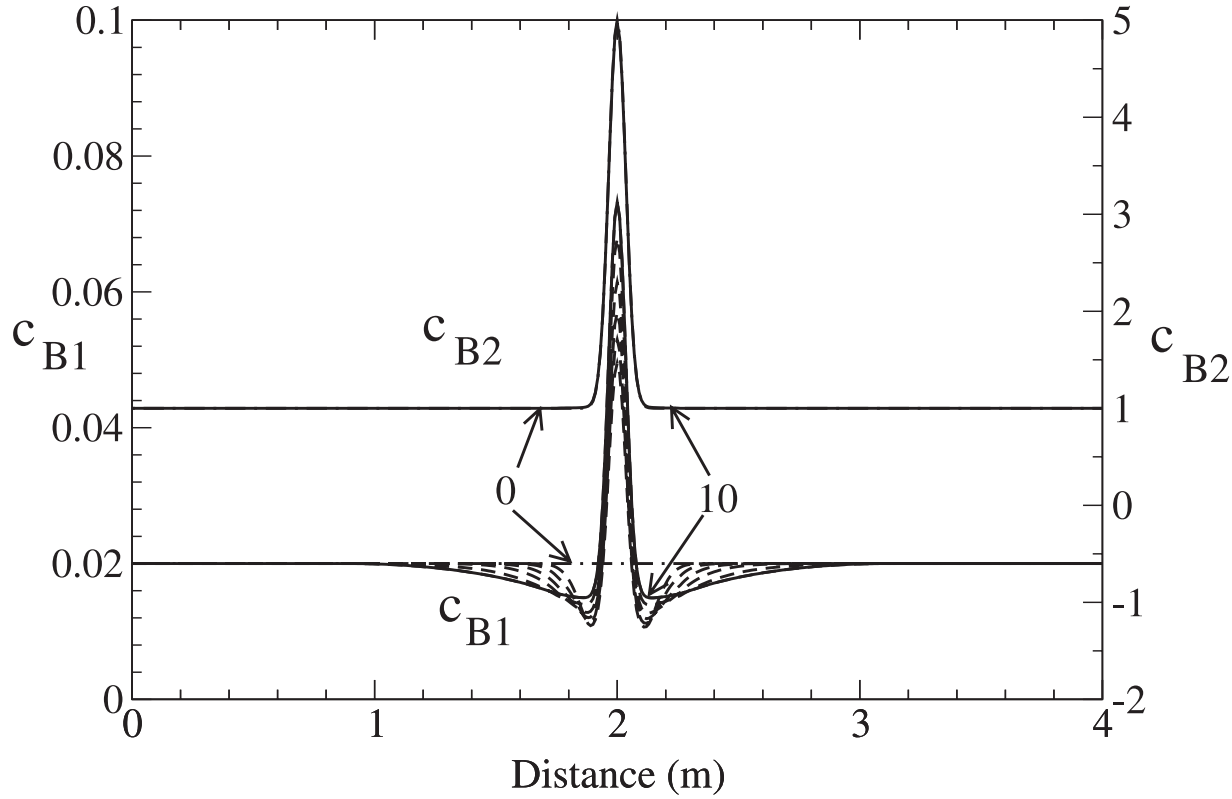

Figure 6. The evolution of the c_{B1}-profile shown in Figure 2 when the distribution coefficients are 100 times greater than the minimum liquid fraction along the profile. The heavy dashed line shows the initial bulk concentration profiles and the light dashed lines show the evolution of the signals at time steps that are 100 times greater than those plotted in Figure 2 (i.e. $\tilde{t}$ = 0.25, 0.5, 1, 2, 5, and 10). The c_{B1}-profile is altered much more slowly when a significant proportion of the impurities is not within the liquid veins. The heavy solid lines show that the c_{B1}-profile still contains significant low-concentration "shoulders" at the edges of the sympathetic bulk concentration spike even when $\tilde{t}$ = 10; when the horizontal axis is measured in meters, this represents a time period of about one millennium.

maximal concentrations during the winter months [*Pasteur and Mulvaney*, 2000]. Once the bulk concentrations have adjusted to eliminate the gradients in the chemical loading, further diffusive alteration is driven only by the intergranular concentration gradients that accompany the gradual spatial variations in temperature. These cause the bulk concentration anomalies to slowly migrate relative to the ice toward warmer temperatures without further altering their spatial signatures.

[30] Our model predicts the development of a "sympathetic" bulk concentration anomaly in response to an elevated bulk concentration of a second component. Comparing the relatively short time period required for this adjustment in the bulk concentration profiles with the much longer time period over which the Eemian isotopic events at GRIP are inferred to have been in place, we conclude that the bulk concentration records require that a significant fraction of the impurity molecules be located outside the liquid network in these core samples. We have presented a theoretical framework that addresses this complication by using an effective distribution coefficient to account for the fraction of each impurity species that is outside the liquid network. When the distribution coefficients of each species are similar in size, the diffusive alteration to the bulk concentration profiles is slowed, but results in the same steady state bulk concentration profiles as when all the impurities are confined to the liquid under isothermal conditions. A more diverse range of behavior is predicted when the distribution coefficients differ significantly. Continued progress in improving the spatial resolution of ice core chemical records will provide a context in which to further explore these interactions, and highlight the importance of quantitative laboratory experiments as complementary tools in climate research.

[31] **Acknowledgments.** We thank Richard Alley, Ian Baker, Gerardo Gross, Sigfus Johnsen, Roland Souchez, Johannes Weertman, Eric Wolff, and Grae Worster for discussions and correspondence that has influenced this work. We also thank Ian Baker and Piers Barnes for providing us with preprints. This research is supported by NSF grant OPP9908945.

References

Alley, R. B., A. J. Gow, S. J. Johnsen, J. Kipfstuhl, D. A. Meese, and Th. Thorsteinsson, Comparison of deep ice cores, *Nature*, *373*, 393–394, 1995.

Baker, I., and D. Cullen, The structure and chemistry of 94m GISP2 ice, *Ann. Glaciol.*, *35*, in press, 2002.

Barnes, P. R. F., R. Mulvaney, E. W. Wolff, and K. Robinson, A technique for the examination of polar ice using the scanning electron microscope, *J. Microsc.*, *205*, 118–124, 2002a.

Barnes, P. R. F., R. Mulvaney, K. Robinson, and E. W. Wolff, Observations of polar ice from the Holocene and the glacial period using the scanning electron microscope, *Ann. Glaciol.*, *35*, in press, 2002b.

dela Chapelle, S., O. Castelnau, V. Lipenkov, and P. Duval, Dynamic recrystallization and texture development in ice as revealed by the study of deep ice cores in Antarctica and Greenland, *J. Geophys. Res.*, *103*, 5091–5105, 1998.

Chappellaz, J., E. Brook, T. Blunier, and B. Malaizé, CH_4 and $\delta^{18}O$ of O_2 records from Antarctic and Greenland ice: A clue for stratigraphic disturbance in the bottom part of the Greenland Ice Core Project and Greenland Ice Sheet Project ice cores, *J. Geophys. Res.*, *102*, 26,547–26,557, 1997.

Cullen, D., and I. Baker, The chemistry of grain boundaries in Greenland ice, *J. Glaciol.*, *46*, 703–706, 2000.

Cullen, D., and I. Baker, Observations of impurities in ice, *Microsc. Res. Tech.*, *55*, 198–207, 2001.

Dash, J. G., H. Fu, and J. S. Wettlaufer, The premelting of ice and its environmental consequences, *Rep. Prog. Phys.*, *58*, 115–167, 1995.

Fukazawa, H., K. Sugiyama, S. Mae, H. Narita, and T. Hondoh, Acid ions at triple junction of Antarctic ice observed by Raman scattering, *Geophys. Res. Lett.*, *25*, 2845–2848, 1998.

Gross, G. W., and R. K. Svec, Effect of ammonium on anion uptake and dielectric relaxation in laboratory-grown ice columns, *J. Phys. Chem.*, *101*, 6282–6284, 1997.

Johnsen, S. F., et al., The $\delta^{18}O$ record along the Greenland Ice Core Project deep ice core and the problem of possible Eemian climatic instability, *J. Geophys. Res.*, *102*, 26,397–26,410, 1997.

Kreutz, K. J., P. A. Mayewski, L. D. Meeker, M. S. Twickler, S. I. Whitlow, and I. I. Pittalwala, Bipolar changes in atmospheric circulation during the little ice age, *Science*, *277*, 1294–1296, 1997.

Legrand, M., C. Hammer, M. DeAngelis, J. Savarino, R. Delmas, H. Clausen, and S. J. Johnsen, Sulfur-containing species (methanesulfonate and SO_4) over the last climatic cycle in the Greenland Ice Core Project (central Greenland) ice core, *J. Geophys. Res.*, *102*, 26,663–26,679, 1997.

Mader, H. M., The thermal-behaviour of the water-vein system in polycrystalline ice, *J. Glaciol.*, *38*, 359–374, 1992a.

Mader, H. M., Observations of the water-vein system in polycrystalline ice, *J. Glaciol.*, *38*, 333–347, 1992b.

Marion, G. M., and S. A. Grant, FREZCHEM: A chemical-thermodynamic model for aqueous solutions at subzero temperatures, *CRREL Spec. Rep. 94-18*, 37 pp., USACRREL, Hanover, N. H., 1994.

Mulvaney, R., E. W. Wolff, and K. Oates, Sulfuric acid at grain-boundaries in Antarctic ice, *Nature*, *331*, 247–249, 1988.

Nye, J. F., Thermal behaviour of glacier and laboratory ice, *J. Glaciol.*, *37*, 401–413, 1991.

Nye, J. F., Water veins and lenses in polycrystalline ice, in *Physics and Chemistry of Ice*, edited by N. Maeno and T. Hondoh, pp. 200–206, Hokkaido Univ. Press, Sapporo, 1992.

Nye, J. F., and F. C. Frank, Hydrology of the intergranular veins in a temperate glacier, in *International Association of Scientific Hydrology Publication 95* (*Symposium at Cambridge 1969: Hydrology of Glaciers*), pp. 157–161, 1973.

Ohtomo, M., and G. Wakahama, Growth-rate of recrystallization in ice, *J. Phys. Chem.*, *87*, 4139–4142, 1983.

Pasteur, E. C., and R. Mulvaney, Migration of methane sulfate in Antarctic firn and ice, *J. Geophys. Res.*, *105*, 11,525–11,534, 2000.

Raymond, C. F., and W. D. Harrison, Some observations on the behavior of the liquid and gas phases in temperate glacier ice, *J. Glaciol.*, *14*, 213–233, 1975.

Rempel, A. W., The dynamics of premelted films: With geophysical applications, Ph.D. thesis, 226 pp., Univ. of Cambridge, Cambridge, 2000.

Rempel, A. W., E. D. Waddington, J. S. Wettlaufer, and M. G. Worster, Premelting and anomalous diffusion in ancient polar ice, *Nature*, *411*, 568–571, 2001a.

Rempel, A. W., J. S. Wettlaufer, and M. G. Worster, Interfacial premelting and the thermomolecular force: Thermodynamic buoyancy, *Phys. Rev. Lett.*, *87*, 088501, 2001b.

Souchez, R., The buildup of the ice sheet in central Greenland, *J. Geophys. Res.*, *102*, 26,317–26,323, 1997.

Souchez, R., M. Lemmens, and J. Chappellaz, Flow-induced mixing in the GRIP basal ice deduced from the CO_2 and CH_4 records, *J. Geophys. Res.*, *22*, 41–44, 1995.

Steffensen, J. P., H. B. Clausen, C. U. Hammer, M. Legrand, and M. De Angelis, The chemical composition of cold events within the Eemian section of the Greenland Ice Core Project ice core from Summit, *Greenland*, *102*, 26,747–26,754, 1997.

Thorsteinsson, T., J. Kipfstuhl, and H. Miller, Textures and fabrics in the GRIP ice core, *J. Geophys. Res.*, *102*, 26,583–26,599, 1997.

Tiller, W. A., *The Science of Crystallization, Microscopic Interfacial Phenomena*, 391 pp., Cambridge Univ. Press, New York, 1991.

Welch, K. A., P. A. Mayewski, and S. I. Whitlow, Methanesulfonic acid in coastal Antarctic snow related to sea-ice extent, *J. Geophys. Res.*, *20*, 443–446, 1993.

Waddington, E. D., J. F. Bolzan, and R. B. Alley, Potential for stratigraphic folding near ice-sheet centers, *J. Glaciol.*, *47*, 639–648, 2001.

Wettlaufer, J. S., Introduction to crystallization phenomena in natural and artificial sea ice, in *IAPSO Advanced Study Institute-Summer School: Physics of Ice-Covered Seas*, edited by M. Leppäranta, pp. 105–194, Univ. of Helsinki Press, Helsinki, 1998.

Wettlaufer, J. S., Ice surfaces: Macroscopic effects of microscopic structure, *Philos. Trans. R. Soc. London, Ser. A*, *357*, 3403–3425, 1999.

Wettlaufer, J. S., and J. G. Dash, Melting below zero, *Sci. Am.*, *282*, 50–53, 2000.

Wolff, E. W., Location, movement and reactions of impurities in solid ice, in *Chemical Exchange between the Atmosphere and Polar Snow, NATO ASI Ser. I*, vol. 43, edited by E. W. Wolff and R. C. Bales, pp. 541–560, Springer-Verlag, New York, 1996.

Wolff, W., and J. G. Paren, A two-phase model of electrical conduction in polar ice sheets, *J. Geophys. Res.*, *89*, 9433–9438, 1984.

Wolff, E. W., R. Mulvaney, and K. Oates, The location of impurities in Antarctic ice, *Ann. Glaciol.*, *11*, 194–197, 1988.

Worster, M. G., Solidification of fluids, in *Perspectives in Fluid Dynamics*, edited by G. K. Batchelor et al., pp. 393–446, Cambridge Univ. Press, New York, 2000.

Worster, M. G., and J. S. Wettlaufer, The fluid mechanics of premelted liquid films, in *Fluid Dynamics at Interfaces*, edited by W. Shyy and R. Narayanan, pp. 339–351, Cambridge Univ. Press, New York, 1999.

Zielinski, G. A., P. A. Mayewski, L. D. Meeker, K. Gronvold, M. S. Germani, S. Whitlow, M. S. Twickler, and K. Taylor, Volcanic aerosol records and tephrochronology of the Summit Greenland, ice cores, *J. Geophys. Res.*, *102*, 26,625–26,640, 1997.

A. W. Rempel, Department of Geology and Geophysics, Yale University, New Haven, CT 08620-8109, USA. (alan.rempel@yale.edu)

E. D. Waddington, Department of Earth and Space Sciences, University of Washington, Box 351310, Seattle, WA 98195-1310, USA.

J. S. Wettlaufer, Department of Geology and Geophysics, Yale University, Box 208109, New Haven, CT 06520-8109, USA.